

# Cyclic behaviour of end-plate beam-to-column composite joints

Rui Simões† and Luís Simões da Silva‡

*Departamento de Engenharia Civil, Universidade de Coimbra,  
Polo II, Pinhal de Marrocos, 3030 Coimbra, Portugal*

Paulo J.S. Cruz†

*Departamento de Engenharia Civil, Universidade do Minho,  
Azurém, 4800-058 Guimarães, Portugal*

**Abstract.** An experimental research program on end-plate beam-to-column composite joints under cyclic loading is presented. The major focus relates to the identification of the contribution of the concrete confinement in composite columns to the behaviour of the joint, on internal nodes and external nodes, together with an assessment of degradation of strength and stiffness in successive loading cycles. From the experimental results it was possible to identify the various failure modes and to fit the corresponding hysteretic curves to the Richard-Abbott and Mazzolani models. These curve-fitting exercises highlighted the need to adapt both models, either for improved ease of application, or to deal with some aspects previously not covered by those models.

**Keywords:** composite joints; cyclic behaviour; end-plate; composite columns; hysteretic curves.

---

## 1. Introduction

The behaviour of joints under cyclic loading, when compared to the corresponding static monotonic response, presents the added difficulty of degradation of strength and stiffness in successive loading cycles. Composite joints in seismic regions must provide adequate performance under load reversal, with good energy dissipation. To try to provide some additional insight into this problem, an experimental research program on end-plate beam-to-column composite joints under cyclic loading carried out at the University of Coimbra is described in this paper.

A review of research in this field shows that in the last few years knowledge of the behaviour of beam-to-column composite joints has advanced extraordinarily. Experimental research on the behaviour of composite joints under cyclic loading can be traced back to 3 tests performed by Ammerman and Leon that revealed good behaviour of composite joints under cyclic loads. Table 1 summarises the major experimental research projects carried out until 1998, performed by Lee and Lu (1989), Sheikh *et al.* (1989), Leon (1990), Benussi and Zandonini (1991), Plumier and Schleich (1993), Pradhan and Bouwkamp (1994), Amadio *et al.* (1994), Ermopoulos *et al.* (1995) and Leon *et al.* (1998).

---

†Assistant Professor

‡Associate Professor

Table 1 Tests in composite joints under cyclic loads

Authors (date)	No of tests	Description	Main parameters investigated
Lee and Lu (1989)	3	Tests in composite joints: 2 in external node (minor and major axis) and 1 in internal node.	Evaluation of strength, stiffness, ductility and energy dissipation capacity.
Sheikh <i>et al.</i> (1989)	8	Tests in joints between steel beams and composite or concrete columns.	Evaluation of strength and stiffness; confinement effect of stirrups in the nodal zone.
Leon (1990)	7	Tests in internal nodes with several steel details.	Seismic performance
Benussi & Zandonini (1991)	-	Composite joints with end plate and flange cleats.	Seismic performance
Plumier & Schleich (1993)	48	38 tests in composite joints, being 18 in external nodes and 20 in internal nodes and 10 tests in complete frames.	Global behaviour
Pradhan & Bouwkamp (1994)	-	Cyclic and pseudo-dynamic tests in composite joints	End-plate joints; welded joints; different column web tickness and confinement effect in columns.
Amadio <i>et al.</i> (1989)	-	Cyclic and dynamic tests in composite frames with several types of joints.	Seismic performance
Ermopoulos <i>et al.</i> (1995)	2	Tests of joints between composite beams and composite columns in internal nodes.	Effect of confinement in columns.
Leon (1998)	2	Composite joints	Effect of slab

Based on the results of the experiments described above and some additional research projects on cyclic behaviour of steel joints carried out by Popov (1988), Korol *et al.* (1990), Bernuzzi *et al.* (1996), Calado (1995, 1996) and Calado and Lamas (1998), it can be concluded that (Simões 2000):

– In general, composite structures with semi-rigid joints present adequate behaviour under seismic loads in areas of low to moderate seismicity, being an economical solution for buildings up to 6 storeys (Leon 1990).

– In general, composite joints exhibit stable cyclic behaviour, although the relevant mechanical properties (moment resistance, stiffness and rotation capacity) are invariably lower than those obtained under monotonic loading. For most of the tested joints, the degradation of properties was more pronounced in the negative moment zone (negative bending moments) (Elnashai *et al.* 1995).

– To achieve adequate behaviour under cyclic loading, joints must exhibit high ductility and energy dissipation; this can be achieved by ensuring that the brittle components such as bolts and welds have higher resistance than the ductile components (Plumier 1994, Plumier and Schleich 1993). For the joints tested by Leon *et al.* (1998), failure was always brittle corresponding to low-cycle fatigue of the welds connecting the bottom beam flange to the column flange.

– The overstrength rule of joints with respect to the connected members imposed by Eurocode 8 is rarely observed in composite joints, particularly when subjected to positive bending moment (Elnashai *et al.* 1995).

– The deformability of the column web panel in shear contributes significantly to the energy dissipation of a joint (Plumier 1994), given its high ductility; in a composite joint, the reinforced concrete slab increases the strength and stiffness of the column web because of an increase of lever arm

(Lee and Lu 1989).

– In a composite joint where the column web panel is involved in concrete (composite column), strength and stiffness are considerably increased (Pradhan and Bouwkamp 1994); concrete, even when cracked, provides a significant contribution (Plumier and Schleich 1993). However, according to Elnashai *et al.* (1995), the contribution of concrete is only effective for static monotonic loading; for cyclic loading, the contribution of the concrete involving the column web should not be considered, unless effective confinement is provided.

– For most of the cyclic tests performed on composite beam-to-column joints, distinct behaviour is observed under positive and negative bending moments, mostly because composite joints are usually asymmetrical with respect to the horizontal centroidal axis. In general, the maximum negative bending moment is higher than the positive moment (Ermopoulos *et al.* 1995).

– In a composite joint, the degradation of mechanical properties is primarily related to the components that depend on concrete (Lee and Lu 1989).

– Whenever the degradation of the properties of a joint is linked to the ovalization of bolt holes in shear (top and seat bolted joints) or cracking of concrete (column-slab interaction zone), the resulting cyclic behaviour is characterized by hysteretic curves with slippage (Calado 1995).

The cyclic behaviour of a joint is always unstable, exhibiting a progressive degradation of its mechanical properties: strength, stiffness and energy dissipation capacity (Simões 2000). In seismic areas, characterised by repeated load reversal, the resulting joint response should remain as symmetrical as possible, an imposition much harder to ensure in common beam-to-column composite joints, given the asymmetry of the joint with respect to the centroidal axis.

Hysteretic moment-rotation curves are usually adopted to reproduce the observed behaviour under cyclic loading, based on various alternative mathematical models proposed in the literature (Chui and Chan 1996). These mathematical descriptions of hysteretic behaviour depend on several parameters that allow good adjustment to the experimental curves. To fully predict the behaviour of composite joints under cyclic loading, these parameters should ideally be obtained from known mechanical properties under static loading.

It is the objective of this paper to present a series of experimental test results that will be used to widen and validate current methodologies for the analysis of steel and composite joints. Additionally, the various failure modes corresponding to the tested internal and external node configurations, with and without composite columns, are identified. These results are discussed within the framework of the Richard-Abbott and Mazzolani hysteretic models, leading to the proposal of modified models to deal with the asymmetry of response and the various required parameters suitable for end-plate beam-to-column composite joints.

## 2. Analytical evaluation of the dynamic behaviour

### 2.1. Richard-Abbott model

The Richard-Abbott model is based on a formula developed in 1975 (Elsati and Richard 1996) to reproduce the elastic-plastic behaviour of several materials and was initially used to simulate the static monotonic response of joints and later applied to cyclic situations (De Martino *et al.* 1984). According to this model, the loading branch of the moment-rotation curve of a joint is described by Eq. (1).

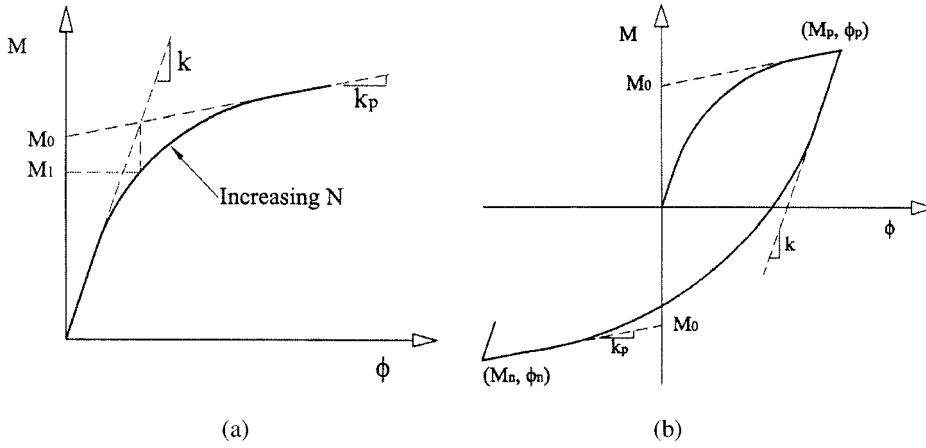


Fig. 1 Richard-Abbott model. (a) Loading branch, (b) Loading-unloading curve

$$M = \frac{(k - k_p) \cdot \phi}{\left[ 1 + \left| \frac{(k - k_p) \cdot \phi}{M_0} \right|^{1/N} \right] + k_p \cdot \phi} \tag{1}$$

Parameters  $k$ ,  $k_p$  and  $M_0$  are defined in Fig. 1a, while  $N$  may be related with these parameters by the following equation:

$$N = \frac{-\ln 2}{\ln \left( \frac{M_1}{M_0} - \frac{k_p}{k - k_p} \right)} \tag{2}$$

The tangent to the curve at a generic point is defined by the following equation, obtained after differentiation of Eq. (1):

$$K_\phi = \frac{dM}{d\phi} = \frac{(k - k_p)}{\left[ 1 + \left| \frac{(k - k_p) \cdot \phi}{M_0} \right|^{1/N} \right]^{\frac{N+1}{N}}} + k_p \tag{3}$$

The unloading branch of the curve is described by a similar equation, starting from point  $(M_p, \phi_p)$ , as described in Fig. 1b.

$$M = M_p - \frac{(k - k_p) \cdot (\phi_p - \phi)}{\left[ 1 + \left| \frac{(k - k_p) \cdot (\phi_p - \phi)}{2 \cdot M_0} \right|^{1/N} \right] - k_p \cdot (\phi_p - \phi)} \tag{4}$$

Subsequent loading curves can be obtained from Eq. (4), replacing the point with coordinates  $(M_p, \phi_p)$  by the new inversion point, with  $(M_n, \phi_n)$  coordinates, and so forth.

The previous equations consider a similar response for hogging and sagging moments. In asymmetrical joints with respect to the centroidal axis, as is the present case of composite joints, the

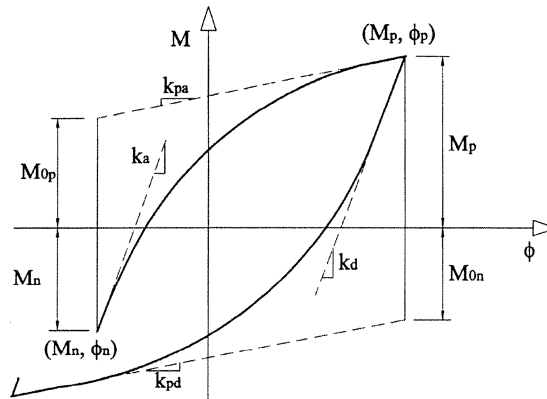


Fig. 2 Richard-Abbott model, adapted to deal with different behaviour under positive and negative bending

previous equations may be modified according to Fig. 2. The loading curve for a generic branch is now given by the following equation:

$$M = M_n - \frac{(k_a - k_{pa}) \cdot (\phi_n - \phi)}{\left[ 1 + \left| \frac{(k_a - k_{pa}) \cdot (\phi_n - \phi)}{M_{0a}} \right|^N \right]^{1/N}} - k_{pa} \cdot (\phi_n - \phi) \quad (5)$$

where  $M_{0a} = M_n + M_{0p}$ . The unloading curve is obtained in the same way, replacing  $(M_n, \phi_n)$  by  $(M_p, \phi_p)$  and the parameters  $M_{0a}$ ,  $k_a$  and  $k_{pa}$  by the corresponding values evaluated at unloading,  $M_{0d}$ ,  $k_d$  and  $k_{pd}$ .

In general, whenever a joint is subjected to successive loading cycles in plastic regime, parameters  $k$ ,  $k_p$ ,  $M_0$  and  $N$  (either for the loading or unloading branches) does not remain constant. In particular, stiffness  $k$  and moment  $M_0$  exhibit a tendency to reduce, corresponding to the degradation of the mechanical properties of the joint.

## 2.2. Modified Mazzolani model

The model proposed by Mazzolani (De Martino *et al.* 1984, Mazzolani 1988), based on the Ramberg-Osgood model, allows the mathematical simulation of hysteretic behaviour with slippage, where the cycles have the shape shown in Fig. 3. As originally proposed, each complete cycle was divided in four branches (I, II, III and IV), the definition of branches I and II being similar to branches III and IV. However, in unsymmetrical joints, all parameters must be defined separately for the positive (branches I and II) and negative (branches III and IV) zones.

Given that, in joints with slippage, the corresponding branch may start in the unloading zone (Fig. 4), thus preventing the application of the model, a modified version is proposed in this paper. It consists of the definition of each cycle with two single branches, ascending and descending, as described in Fig. 5, thus eliminating the limitation of slippage not being able to occur in the unloading branch.

The mathematical description of the ascending branch I ( $M_n \leq M \leq M_p$ ) is given by Eqs. (6a) to (6c). The initial rotation ( $\phi_n$ ) and initial stiffness ( $R$ ) are evaluated at point  $(M_n, \phi_n)$ :

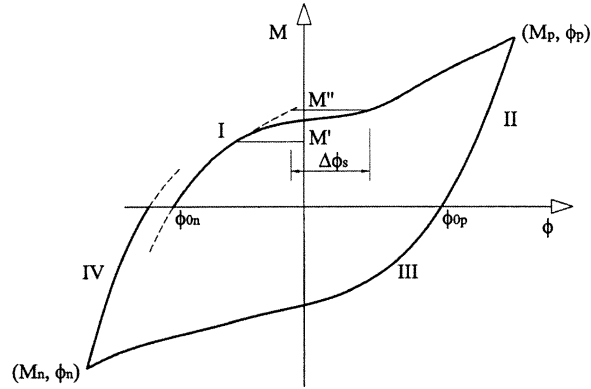


Fig. 3 Definition of a complete cycle according to the Mazzolani model

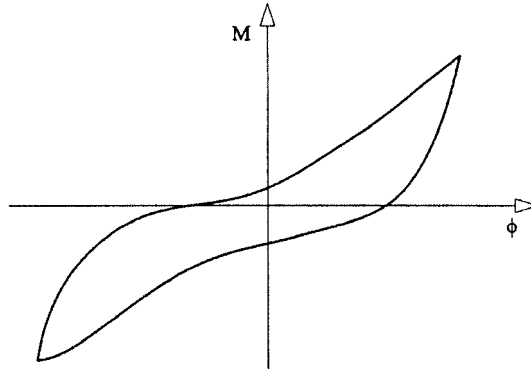


Fig. 4 Hysteretic curve with the slippage branch starting in the unloading zone

$$\phi = \phi_n + \frac{M - M_n}{R} + c_1 \cdot \left( \frac{M - M_n}{M_2} \right)^{c_2} \quad M_n \leq M \leq M' \quad (6a)$$

$$\phi = \phi_n + \frac{M - M_n}{R} + c_1 \cdot \left( \frac{M - M_n}{M_2} \right)^{c_2} + \frac{\Delta\phi_s}{2} + \left( \frac{\Delta\phi_s}{2} - K_m \right) \cdot \rho \cdot |\rho|^{s-1} + K_m \cdot \rho \quad \text{if } M' \leq M \leq M'' \quad (6b)$$

$$\phi = \phi_n + \frac{M - M_n}{R} + c_1 \cdot \left( \frac{M - M_n}{M_2} \right)^{c_2} + \Delta\phi_s \quad \text{if } M'' \leq M \leq M_p \quad (6c)$$

Moment  $M_2$  is used to constrain the curve to an intermediate point, defined in the context of the present work as a rotation of the order of 1.25 the elastic rotation, so that this point lies outside the slippage branch. Parameters  $c_1$  and  $c_2$  are obtained from Eqs. (7) and (8).

$$c_1 = 0.25 \cdot \phi_y = 0.25 \cdot \frac{M_2}{R} \quad (7)$$

$$c_2 = \frac{\ln \left[ \left( \phi_{lim} - \frac{M_{lim}}{R} \right) / c_1 \right]}{\ln(M_{lim}/M_2)} \quad (8)$$

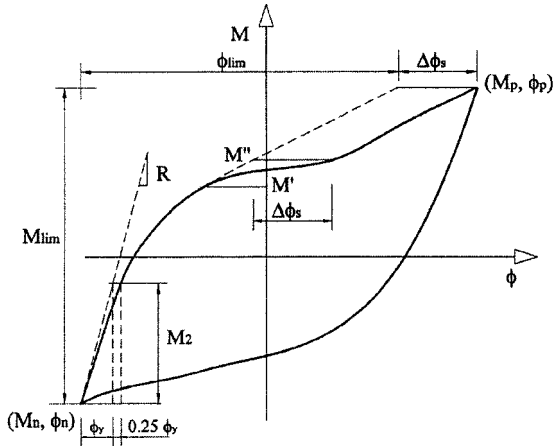
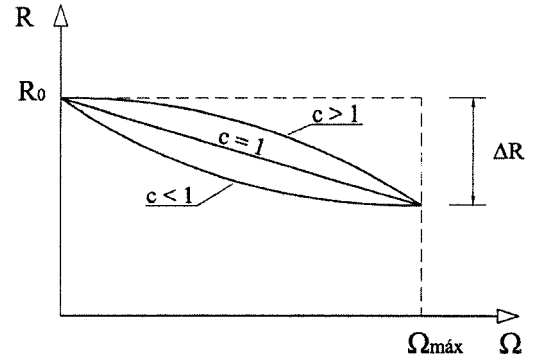


Fig. 5 Definition of a complete cycle


 Fig. 6 Tangent to the  $M-\phi$  curve as a function of the accumulated energy

where  $M_{lim} = |M_n| + |M_p|$  and  $\phi_{lim} = |\phi_n| + |\phi_p| - \Delta\phi_s$ .

The stiffness at the start of each cycle ( $R$ ) is obtained as a function of the accumulated energy of the previous cycle ( $\Omega$ ), according to Eq. (9), as shown in Fig. 6.

$$R = R_0 \cdot \left[ 1 - \frac{\Delta R}{R_0} \cdot \left( \frac{\Omega}{\Omega_{\max}} \right)^c \right] \quad (9)$$

where:

$R_0$ -Tangent in the beginning of the first cycle, obtained from the static monotonic moment-rotation results;

$\Delta R$ -Tangent variation, between the first and last cycle before collapse;

$\Omega$ -Accumulated energy at the end of the previous cycle;

$\Omega_{\max}$ -Accumulated energy at collapse;

$c$ -Parameter defined according to Fig. 6.

Eq. (6b) results from adding the slippage effect between  $M'$  and  $M''$  to Eq. (6a). The second part of Eq. (6b) is defined in terms of the slippage  $\Delta\phi_s$  and the parameters  $\rho$ ,  $s$  and  $K_m$ . The parameter  $\rho$  is related to the bending moments  $M$ ,  $M'$  and  $M''$  through Eq. (10).

$$\rho = \frac{2 \cdot M - M' - M''}{M'' - M'} \quad (-1 < \rho < 1 \text{ for } M' < M < M'') \quad (10)$$

Parameters  $K_m$  and  $s$  ensure continuity at points  $M = M'$  and  $M = M''$  (Fig. 7).

$$s = \frac{K_m}{K_m - \Delta\phi_s/2} \quad \text{with } K_m > \Delta\phi_s/2 \quad (11)$$

Assuming that slippage  $\Delta\phi_s$  varies from cycle to cycle, it could be related to the accumulated energy  $\Omega$  until the previous cycle, through equation:

$$\Delta\phi_s = \Delta\phi_{s, \min} + (\Delta\phi_{s, \max} - \Delta\phi_{s, \min}) \cdot \left(\frac{\Omega}{\Omega_{\max}}\right)^g \quad (12)$$

where:

- $\Delta\phi_{s, \min}$  - Slippage in the first cycle;
- $\Delta\phi_{s, \max}$  - Slippage in the last cycle before failure;
- $g$  - Adjust parameter.

Finally Eq. (6c) expresses the hysteretic behaviour after slippage, obtained through Eq. (6a), by means of a translation corresponding to slippage  $\Delta\phi_s$ .

Starting from the positive extremum of the previous half-cycle, the descending branch is defined in a similar fashion.

To reproduce the strength degradation in the current model, a degradation curve is proposed for  $M_{lim}$  similar to the one considered for stiffness ( $R$ ). Starting from an initial value, the current value for a given cycle is given by:

$$M_{lim} = M_{lim0} \cdot \left[ 1 - \frac{M_{lim}}{M_{lim0}} \cdot \left(\frac{\Omega}{\Omega_{\max}}\right)^p \right] \quad (13)$$

where:

- $M_{lim0}$  - Initial  $M_{lim}$ , obtained from the static monotonic moment-rotation results;
- $\Delta M_{lim}$  - between  $M_{lim}$  evaluated at the first and last cycle before collapse;
- $\Omega$  - Accumulated energy at the end of the previous cycle;
- $\Omega_{\max}$  - Accumulated energy at collapse;
- $p$  - Parameter defined according to Fig. 8.

In contrast with stiffness,  $M_{lim}$  does not decrease for cycles with amplitudes little greater than the elastic amplitude; on the contrary, from the elastic amplitude ( $\Omega = 0$ ) and up to a certain value, an increase of  $M_{lim}$  is noted. Consequently, Eq. (13) should only be used for cycles of amplitude equal or larger than the maximum attained moment. In the context of the present work, this corresponds to 4 times the elastic amplitude,  $M_{lim}$  being obtained directly from the static monotonic or cyclic envelope of the moment-rotation curve for smaller amplitudes.

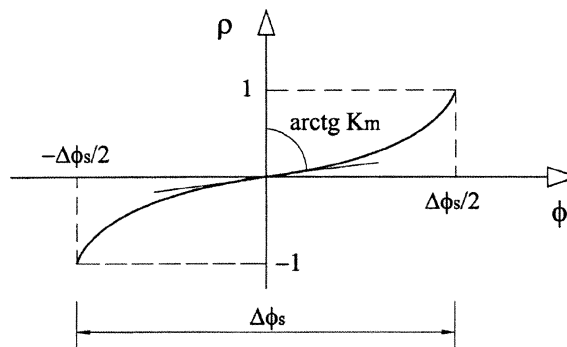


Fig. 7 Part of the  $M$ - $\phi$  curve where slippage occurs

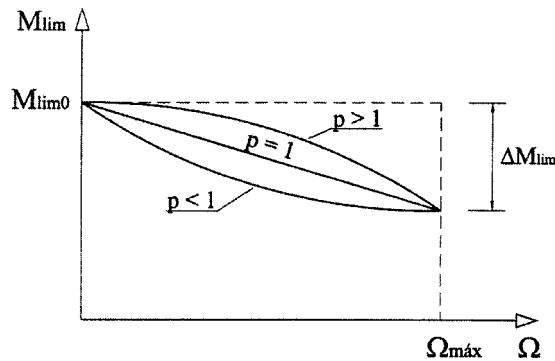


Fig. 8 Relation between  $M_{lim}$  and the accumulated energy (a) Internal node with steel column, (b) External node with composite column

### 3. Test program

The test program performed at the Civil Engineering Department of the University of Coimbra included 4 prototypes, 2 being in internal nodes and 2 in external nodes, a thorough description being found elsewhere (Simões 2000). The description of each model includes the geometric definition, the material properties and the testing and instrumentation procedures.

The prototypes, covering internal and external nodes (Fig. 9), were defined such that they could reproduce the joints in a common framed structure, with spans of about 7 m, 4 m spacing between frames, live loads up to 4 kN/m<sup>2</sup> and a high energy dissipation capacity and a good fire resistance (ENV 1993-1-1, 1992, ENV 1994-1-1 1996). According to the objectives of this study, the steel joint is the same in all prototypes, corresponding to a beam connected to the column by one end plate, welded to the beam and bolted to the column.

In all cases, the beams consist of an IPE 270, rigidly connected to a reinforced concrete slab (full interaction) by 8 shear block connectors. The slab, 900 mm wide and 120 mm thick, is reinforced with 10 $\phi$ 12 longitudinal bars and 10 $\phi$ 8 transversal bars per meter, with 20 mm cover. The steel joint consists of a 12 mm thick end-plate, welded to the beam and bolted to the column flange through 6 M20 bolts (class 8.8). The end-plate is flushed at the top and extended at the bottom, in order to achieve similar behaviour under positive and negative moments. The steel column is the same in all the tests (HEA 220), being encased by concrete (300 $\times$ 300 mm) in tests E10 and E12, with longitudinal reinforcement of 4 $\phi$ 12, with one bar in each corner of the section and stirrups consisting of  $\phi$ 6 bars 0.08 m apart. The following materials were chosen: S235 in the steel components, steel class 8.8 in the bolts, steel A400 NR in the reinforcing bars.

The loads were applied to the beams 1.40 m from the steel column face with two dynamic actuators with a capacity of 200 kN and 600 kN, and maximum displacement of 20 cm and 10 cm, respectively.

The instrumentation of the specimens was carried out in order to make possible the evaluation of the main mechanical properties and the strain and stress levels of the fundamental components.

Several measuring instruments were used in order to evaluate the contribution of each component to the global behaviour of the joints: displacement transducers (LVDT's), unidirectional extensometers,

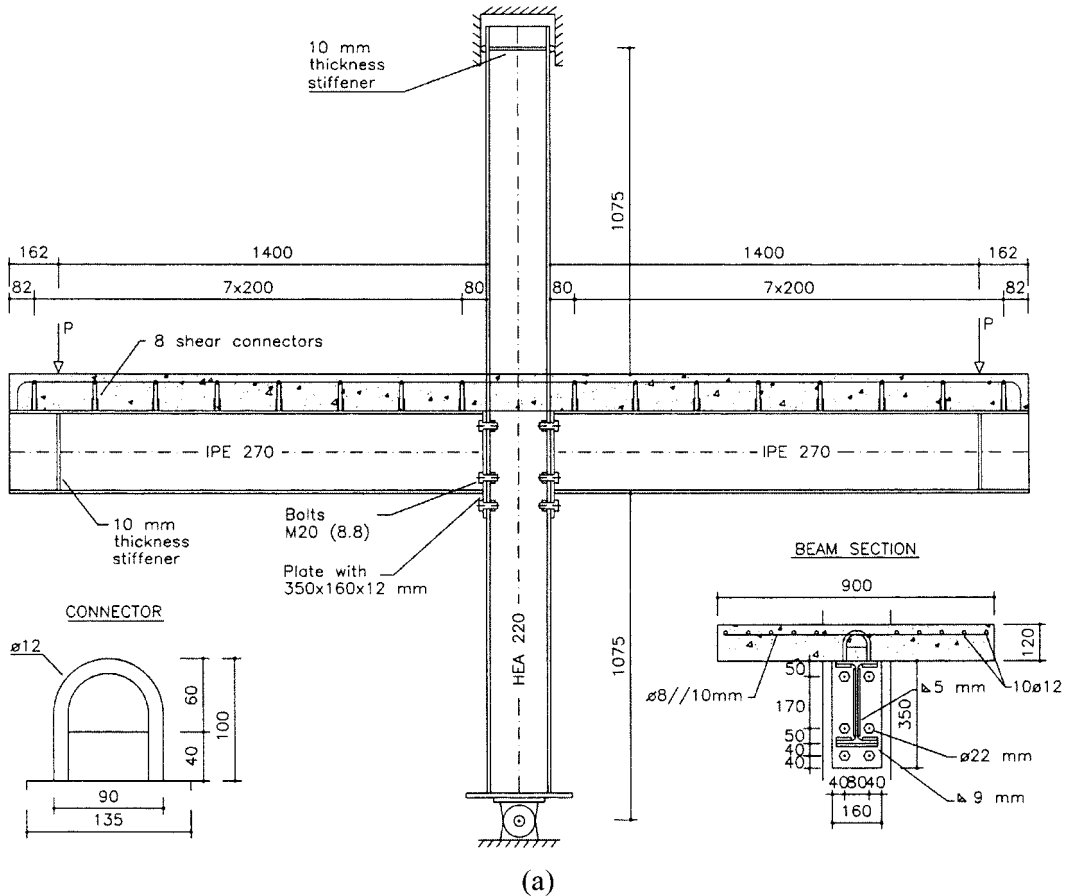


Fig. 9 Experimental models for internal and external nodes

rosettes, load cells and manual inclinometers. The evaluation and recording of all the measured values was done with an acquisition system-TDS601-TML.

In both tests, loading was applied according to the methodology proposed by the ECCS (1986), as shown in Fig. 10, with both joints (left and right) being equally loaded but out of phase by one half cycle. Each cyclic test comprised 3 elastic cycles followed by 12 to 15 cycles in plastic range, the elastic displacement being evaluated from the results of earlier equivalent static tests (Simões 2000, Silva *et al.* 2001).

#### 4. Test results

Two tests were performed in internal nodes, test E11 corresponding to the prototype arrangement between composite beams and a steel column, shown in Fig. 9a and test E12 between composite beams and a composite column.

The column web panel, under horizontal shear, was the most influent component of the cyclic

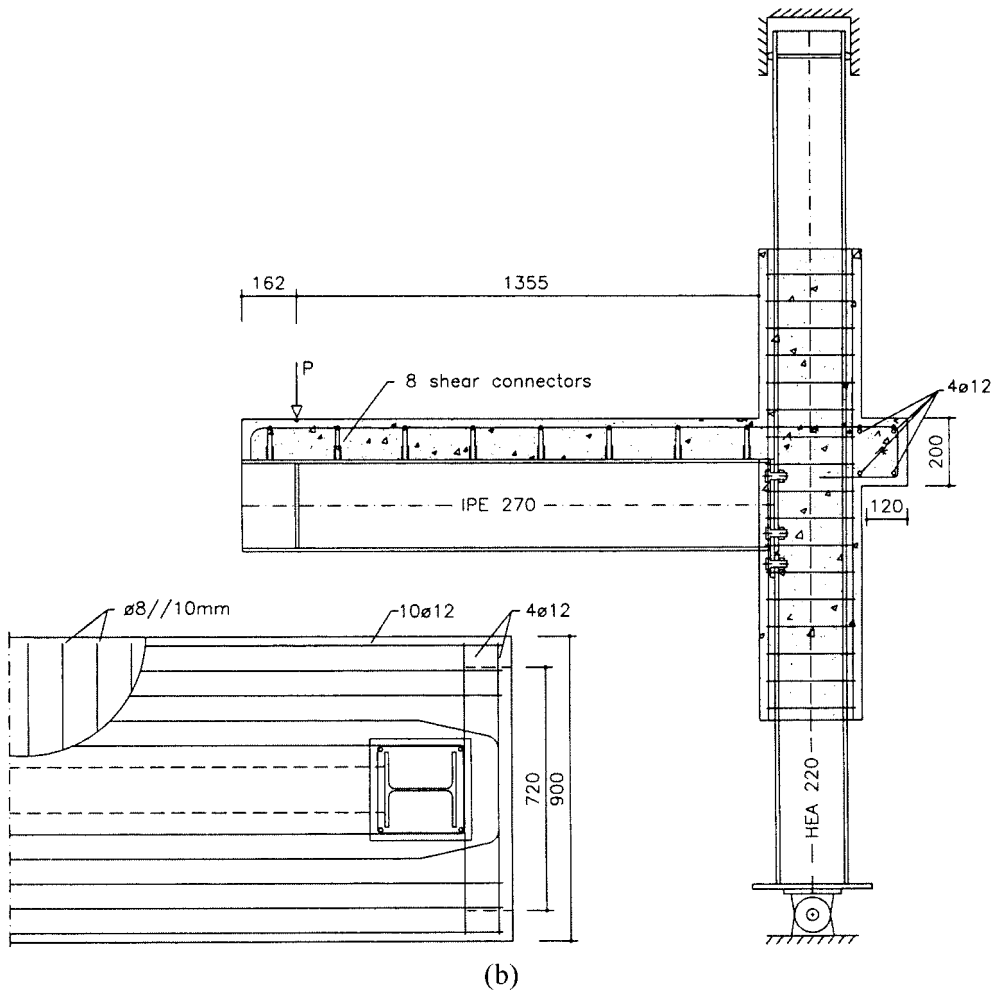


Fig. 9 Continued

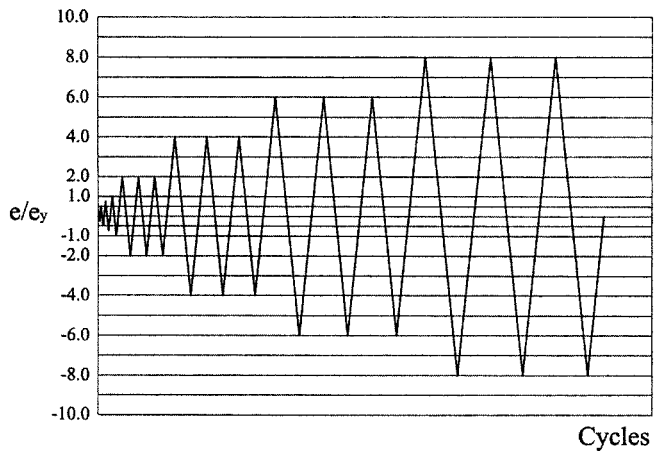


Fig. 10 Displacement amplitudes used in cyclic tests



Fig. 11 Photos of the prototypes after testing (a) Test E11 Steel column, (b) Test E12 Composite column

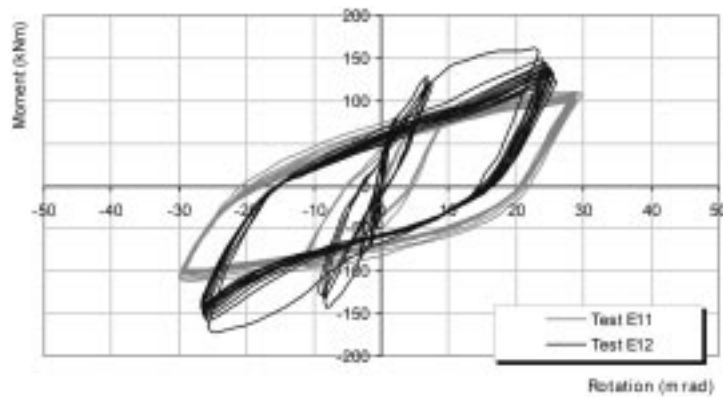


Fig. 12 Hysteretic moment total rotation curves of joints E11 and E12

behaviour in test E11 (Fig. 11a). In this test the rotation was almost exclusively due the panel distortion. That is the reason why the behaviour under positive and negative moments is similar, as shown in Fig. 12. The influence of the concrete crushing at the column-slab interface was significantly smaller.

Owing to the anti-symmetric loading, the column web panel had also an important contribution to the cyclic behaviour of the test E12 (Fig. 11b); this influence was smaller than in test E11, due to the concrete encasement of the web panel.

From the analysis of the hysteretic curve of test E12 presented in Fig. 12, a marked decrease of the maximum bending moment was observed, from the first to the second cycle of maximum amplitude, both in the positive and negative zones. This decrease was almost exclusively due to the cracking of the encasing concrete.

From the analysis of Fig. 12 it can be concluded that the cyclic behaviour of test E12 approaches the behaviour of test E11, as the concrete cracks grow. This fact permits to conclude that in internal joints, where the influence of the shear force in the panel is dominant, the degree of confinement has not a significant influence.

Similarly to the internal nodes, two tests were performed on external nodes (Fig. 13), test E9 corresponding to a steel column and test E10 corresponding to a composite column, the latter shown in

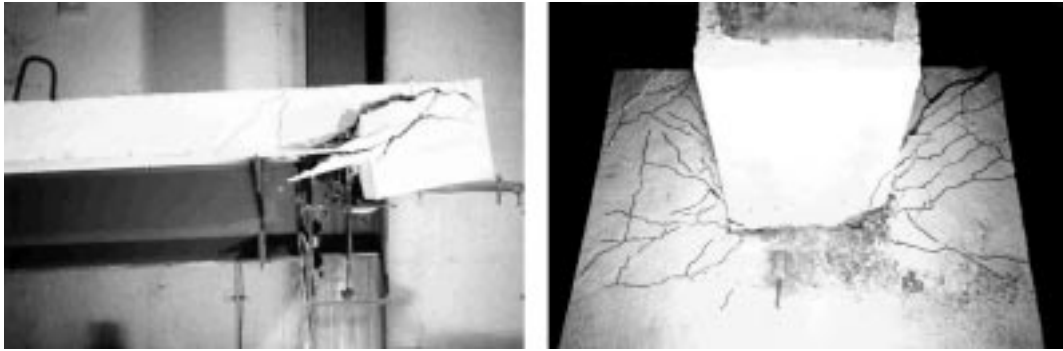


Fig. 13 Photos of the prototypes after testing (a) Test E9 Steel column, (b) Test E10 Composite column

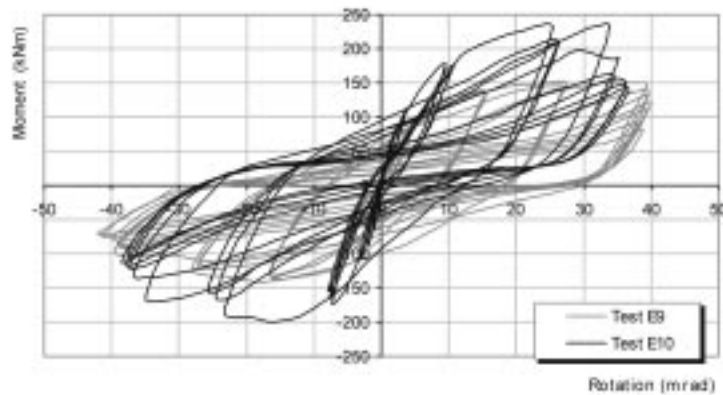


Fig. 14 Hysteretic moment total rotation curves for joints E9 and E10

Fig. 9b. Loading was applied similarly to the internal node tests but with a larger number of amplitudes.

The analysis of the curve shown in the Fig. 14 highlights a strong degradation of the properties of joint E9, when submitted to cyclic loading. The degradation was more obvious in terms of stiffness and dissipated energy; concerning the resistance (maximum bending moment), the degradation was clearer in the cycles of highest amplitude. According to the cycles shape and by inspection of the model before and after each cycle, it was concluded that the properties degradation was caused by slippage in some components.

Considering the asymmetry of the joint with respect to the centroidal axis, the behaviour under hogging and sagging moments was quite different, especially in what concerns to the degradation of resistance. While the degradation of resistance in the positive zone starts after the first cycle of highest amplitude, in the negative zone the maximum bending moment starts to decrease after the first cycle of amplitude  $6e_y$ , even before the maximum amplitude was reached (Fig. 14). This decrease of resistance was clearly due to a reduction in the force developed in the longitudinal slab reinforcement, caused by the cracking of the anchorage zone, with transfer of the tensile force to the first bolt row. This phenomenon is repeated in the first cycle of highest amplitude ( $8e_y$ ).

The contribution of the column web panel distortion to the total joint rotation was quite significant; nevertheless, as it is a component of high ductility, its contribution for the degradation of the joint properties was negligible.

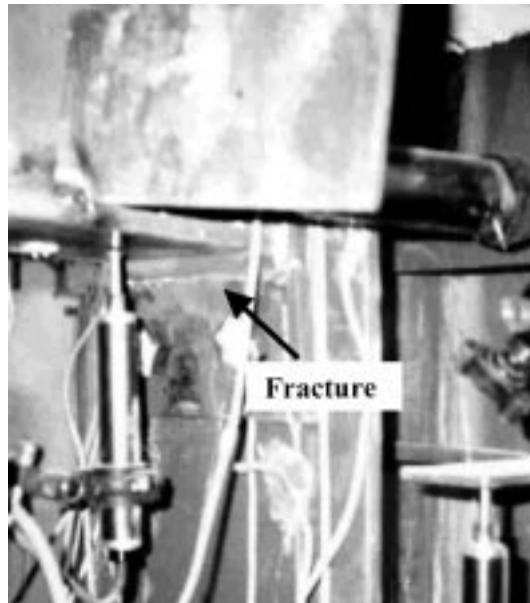


Fig. 15 End-plate fractured (E9)

In test E9 under sagging bending moments (positive zone of the hysteretic curve), the degradation was due to:

- Bending of the end-plate and the column flange in the tension zone, at the bottom flange level (T-Stub). In this zone the bolts were subjected to very high strain levels and end-plate fracture takes place along the bottom edge of the connection to the beam flange, as is shown in Fig. 15;
- Crushing of the compressed concrete in the interface between the slab and the column flange.

In the same test, but under hogging moments (negative zone of the hysteretic curve), the degradation

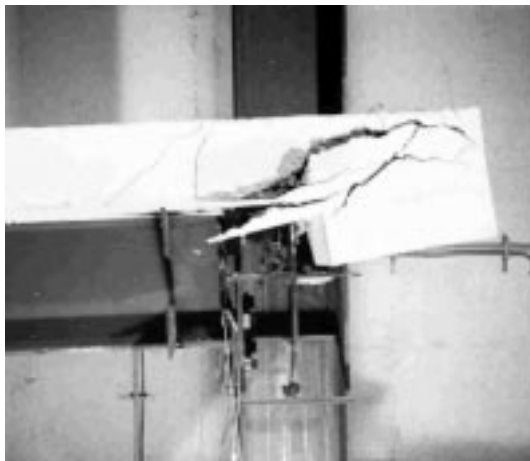


Fig. 16 Concrete cracking (E9)

Table 2 Elastic parameters for tests E9 to E12

Elastic Parameters	$M_{y+}$	$M_{y-}$	$\phi_{y+}$	$\phi_{y-}$	$K_{y+}$	$K_{y-}$
	(kNm)		(mrad)		(kNm/mrad)	
Test E9	114.00	114.99	4.64	4.29	24.57	26.81
Test E10	169.81	158.92	4.60	3.89	36.95	40.83
Test E11	83.41	80.68	5.05	4.28	16.50	18.83
Test E12	116.83	117.78	3.39	3.25	34.44	36.22

was due to:

- Cracking of the slab concrete, conditioned by the anchorage of the longitudinal reinforcement, as it is illustrated in Fig. 16.

The contribution of the column web panel distortion to the total joint rotation in test E10 was not so obvious, when compared to test E9, due to the additional strength provided by the encasing concrete.

Taking as a basis the curves shown in the Fig. 14, it's possible to conclude that the behaviour of both joints was quite different, but only in the cycles of reduced amplitude (close to the elastic zone). For higher amplitudes, since the encasing concrete is cracked, both tests exhibit similar behaviour. This fact confirms the conclusions obtained in the analysis of the cyclic test results for the internal nodes.

The assessment of the cyclic behaviour is performed using parameters obtained from the hysteretic curves. According to the ECCS (1986) definitions, the following parameters were used throughout this work: partial ductility  $\mu_{oi}$ , full ductility  $\mu_i$ , full ductility ratio  $\psi_i$ , resistance ratio  $\varepsilon_i$ , stiffness ratio  $\xi_i$  and absorbed energy ratio  $\eta_i$ .

The moment-rotation curves obtained from static monotonic tests are often considered as the envelope of the cyclic curves. However, this assumption may not well reproduce the reality since, due

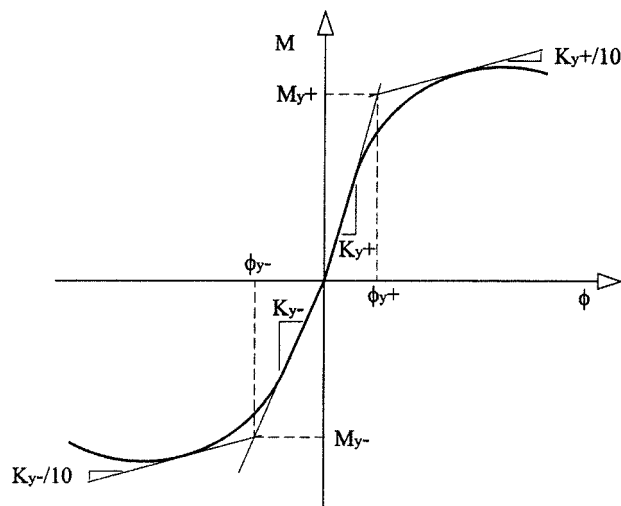


Fig. 17 Elastic parameters

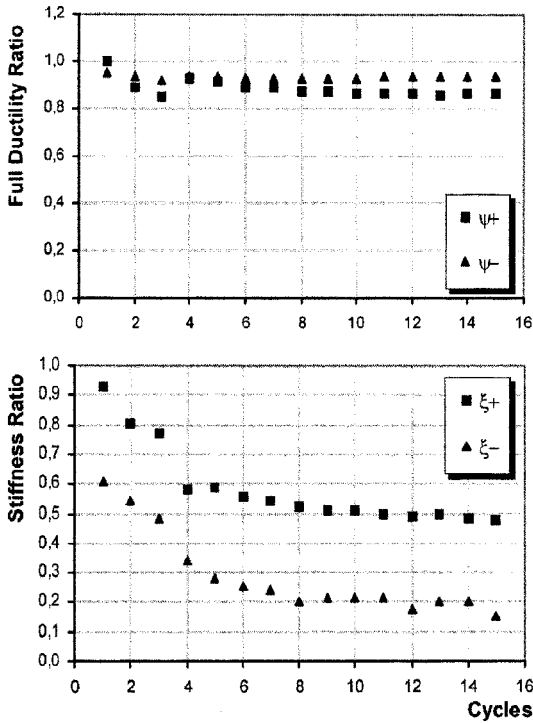


Fig. 18 Full ductility ratio and stiffness ratio in test E11

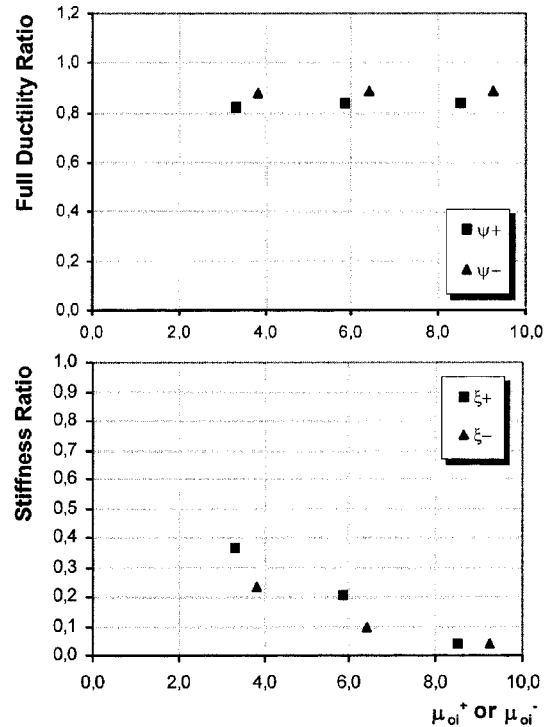


Fig. 19 Full ductility ratio and stiffness ratio in test E9

to steel hardening during cyclic loading, higher bending moments may be reached when compared to the limit established by the static curves.

In tests where the behaviour in the positive and negative zones is different, as in common beam-to-column composite joints subjected to positive and negative bending moments, the elastic parameters must be obtained for both cases. Table 2 describes parameters  $M_{y+}$ ,  $\phi_{y+}$ ,  $K_{y+}$  and  $M_{y-}$ ,  $\phi_{y-}$ ,  $K_{y-}$  corresponding, respectively, to the elastic moment, the elastic rotation and the elastic stiffness, obtained from the positive and negative cycle envelopes, according to Fig. 17.

Due to the limitations of the loading equipment used in the internal node tests, only cycles with two different amplitudes were performed in plastic range. In these cases, the cyclic parameters are graphically presented as a function of the number of cycles, instead of the partial ductility ( $\mu_{oi}$ ) used in the external node tests. As an example, the variation of the full ductility ratio  $\psi_i$  and the rigidity ratio  $\xi_i$  are shown for tests E9 and E11, the remaining being available in (Simões 2000).

For the tests on internal nodes (E11 and E12), the joints presented high ductility (ductility ratio  $\psi_i$  close to unity) (Fig. 18), with similar response for hogging and sagging moment. Because the maximum amplitude was not very high, the strength degradation was low. However, for the stiffness (Fig. 18) and energy degradation ratios, strong reductions were noted (Simões 2000).

For the tests on external nodes (E9 and E10), the ductility ratios remained high (Fig. 19), except for test E10 under negative hogging moment. The strength degradation was severe, while the stiffness ratio (Fig. 19) and energy degradation ratios proved that the joints reached collapse.

## 5. Numerical simulation of the cyclic behaviour

The application of the analytical models described in section 2 to the cyclic behaviour of composite joints (in terms of  $M-\phi$  curves) is presented in this section. The application of these models starts from the experimental (or analytical) static monotonic curves, here defined as the envelopes of the cyclic curves, with the elastic parameters already presented in Table 2 for tests E9 to E12.

Figs. 20 and 21 illustrate the experimental results for the internal node tests, shown superimposed with results from the (a) Richard-Abbott model and (b) the modified Mazzolani model.

Figs. 22 and 23 illustrate the moment-rotation response for the two tests on external nodes, again superimposed with the (a) Richard-Abbott model and (b) the modified Mazzolani model.

The analytical predictions based on the Richard-Abbott model for the cyclic response of the composite joints presented in Figs. 20a to 23a were directly derived from the envelope curves of the cyclic behaviour. Parameter  $k_p$  was taken constant and equal to 5% of the initial elastic stiffness  $k$  (equal to  $K_y^+$  or  $K_y^-$ ). Parameter  $N$  was also kept constant for all cycles and obtained as the average of a previous adjustment cycle by cycle, directly from the experimental results. A decaying law based on the accumulated dissipated energy (obtained analytically) was assumed for parameters  $k$  and  $M_0$ , based on the values obtained for each cycle in the previous section; these curves were calibrated directly from the

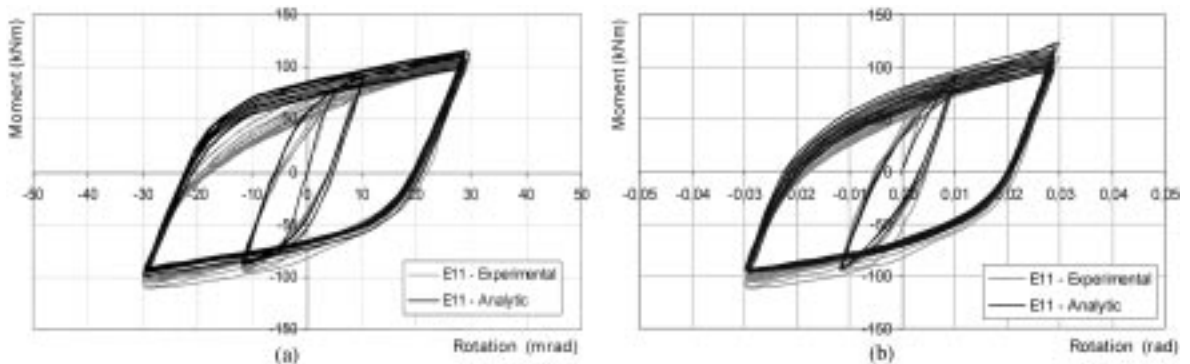


Fig. 20 Moment-rotation response for test E11 (a) Richard-Abbott, (b) Modified Mazzolani

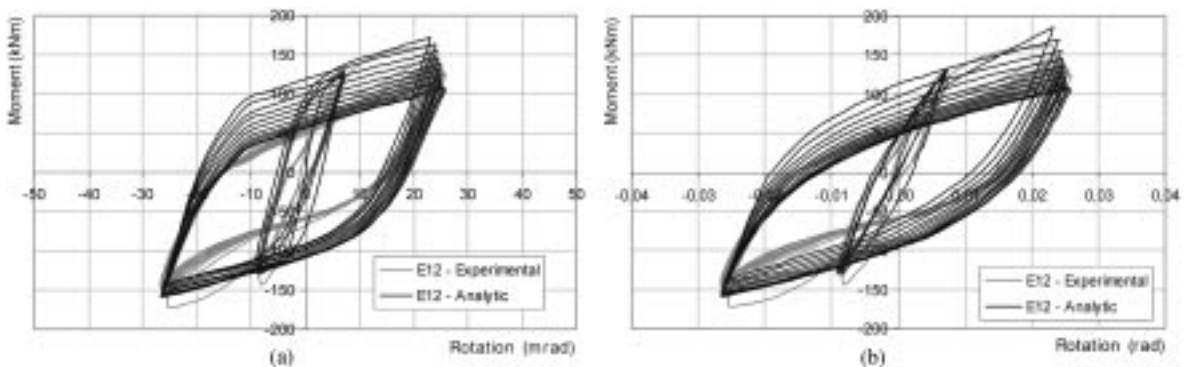


Fig. 21 Moment-rotation response for test E12 (a) Richard-Abbott, (b) Modified Mazzolani

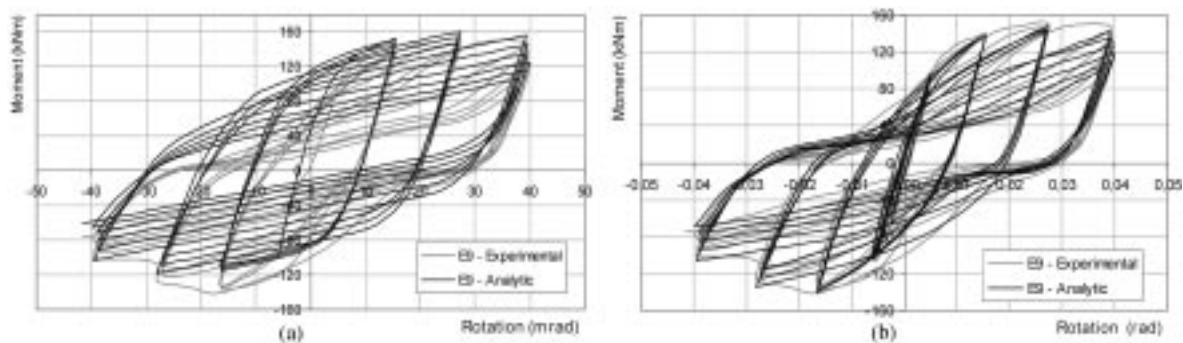


Fig. 22 Moment-rotation response for test E9 (a) Richard-Abbott, (b) Modified Mazzolani

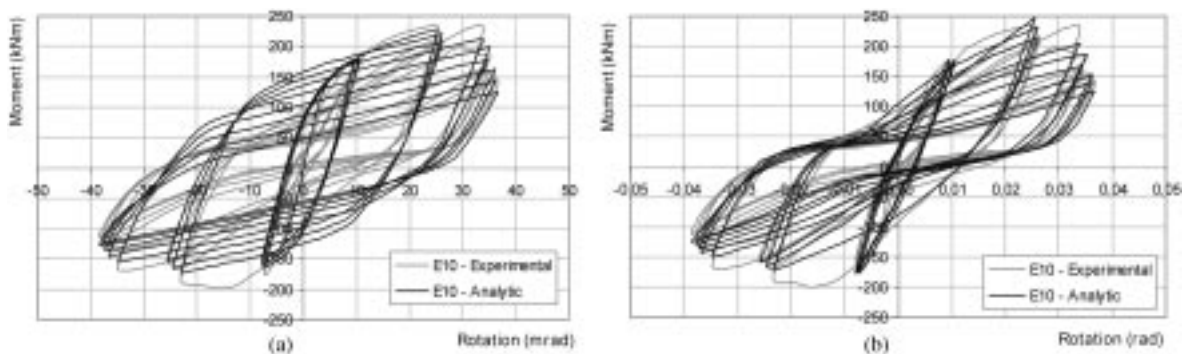


Fig. 23 Moment-rotation response for test E10 (a) Richard-Abbott, (b) Modified Mazzolani

experimental results.

The analytical predictions based on the modified Mazzolani model (Figs. 20b to 23b) also rely on decaying laws for the (i) tangent (stiffness) at the origin of the ascending and descending branches ( $R$ ), (ii) bending moment ( $M_{lim}$ ), and (iii) slippage ( $\Delta\phi_s$ ). These decaying laws are defined from initial values as a function of the accumulated dissipated energy. The initial values of  $R$  and  $M_{lim}$  may be obtained from the envelope curves of the cyclic behaviour; for the remaining parameters, representative values are chosen based on available experimental data.

## 6. Conclusions

From the analysis of the four cyclic tests, all joints presented high ductility ratios ( $\psi_i$ ) and high levels of dissipated energy.

In almost all tests, stiffness was the property with the highest degradation level. The stiffness ratios ( $\xi_i$ ) yields values lower than unity, even for the first cycles in the plastic regime. In terms of resistance, the internal node tests exhibited low degradation levels (stiffness ratios  $\varepsilon_i$  close to unity). Otherwise, for external node tests, due essentially to the concrete cracking observed at the anchorage zone of the slab longitudinal reinforcement, the resistance degradation reached significant levels.

Comparing the cyclic behaviour of the joints with steel columns (E9 and E11) with the same behaviour of the joints with composite columns (E10 and E12), it can be concluded that the differences are not so significant as for the static behaviour, because concrete cracking reduces considerably the advantages of the column web confinement.

The Richard-Abbott model was adjusted so that the error on the maxima moments reached at the end of each half-cycle was minimised. Consequently, agreement between analytical and experimental results for this criterium was good, the maximum difference being obtained for test E9 with +8% difference for positive bending and -10% for negative bending. In terms of energy dissipation, since the Richard-Abbott model cannot adequately reproduce slippage, two distinct situations were observed: for tests E9 and E10, where slippage played a major role, poor agreement was noted between the experimental and the analytical results; for the internal node tests, especially for test E11 where slippage hardly occurred, better agreement was observed, with a total error of +33% and -1% for the positive and negative zones, respectively.

The modified Mazzolani model, with more parameters and able to simulate slippage, gave a much better agreement between experimental and analytical results, particularly with respect to dissipated energy, a crucial aspect in terms of seismic behaviour. In this simulation, some of the parameters were derived from the envelopes of the cyclic curves, calibrated through some coefficients obtained from the experimental evidence available. The error on the evaluation of total dissipated energy was only of 7%. For tests E11 and E12, slippage was not modelled, resulting in an error of +28% for the latter, since some slip was observed on the negative zone. In terms of bending moment, the maximum error occurred for test E10, with an average error of +6%.

Finally, it is noted that the Mazzolani model, with the modifications introduced in this work, constitutes a good tool to predict the cyclic behaviour of joints, particularly beam-to-column composite joints. Its application, however, still requires the calibration of a certain number of coefficients that must be done experimentally. Given that the number of tests used in this work was only 4, all presenting different aspects, its validity should be checked against a wider base of experimental data.

The developments presented in this paper were directed at the daunting task of predicting the dynamic behaviour of steel and composite joints. Although much work still remains to be done, full analytical predictions of the hysteretic response based on the static monotonic behaviour should become possible as soon as the issue of joint ductility and rotation capacity is adequately addressed.

## Acknowledgements

Financial support from “Ministério da Ciências Tecnologia” - PRAXIS XXI research project PRAXIS/P/ECM/13153/1998 is acknowledged.

## References

- Ahmed, B., Li, T.Q. and Nethercot, D.A. (1996), “Modelling composite connection response”, *Connections in Steel Structures III Behaviour, Strength & Design*, ed. R. Bjorhovde, A. Colson and R. Zandonini. Proceedings of the Third International Workshop, Trento University, 29-31 May 1995. Pergamon, Oxford, pp. 259-268.
- Amadio, C., Benussi, F. and Noe, S. (1994), “Behaviour of unbraced semi-rigid composite frames under seismic actions”, In *Behaviour of Steel Structures in Seismic Areas STESSA94*, ed. F. M. Mazzolani and V. Gioncu, E

- & FN SPON, London, pp. 535-546.
- Azevedo, J. and Calado, L. (1994), "Hysteretic behaviour of steel members: analytical models and experimental tests", *J. Constr. Steel Res.*, **29**, 71-94.
- Bernuzzi, C., Zandonini, R. and Zanon, P. (1996), "Experimental analysis and modelling of semi-rigid steel joints under cyclic reversal loading", *J. Constr. Steel Res.*, **38**(2), 95-123.
- Calado, L. (1995), "Experimental research and analytical modelling of the cyclic behaviour of bolted semi-rigid connections", In *Steel Structures Eurosteel95*, ed. A. N. Kounadis, A. A. Balkema, Rotterdam, 197-204.
- Calado, L. (1996), "Low cycle fatigue of beam-to-column connections", COST C1 Earthquake Performance of Civil Engineering Structures, ed. A. Pinto, Luxembourg, 111-122.
- Calado, L. and Lamas, A. (1998), "Seismic modelling and behaviour of steel beam-to-column connections", *J. Constr. Steel Res.*, 46(1-3), Paper n. 267.
- Chui, P.P.T. and Chan, S.L. (1996), "Transient response of moment-resistant steel frames with flexible and hysteretic joints", *J. Constr. Steel Res.*, **39**(3), 221-243.
- De Martino, A., Faella, C. and Mazzolani, F.M. (1984), "Simulation of beam-to-column joint behaviour under cyclic loads", *Costruzioni Metalliche*, **6**, 346-356.
- ECCS. (1986), Recommended Testing Procedure for Assessing the Behaviour of Structural Steel Elements under Cyclic Loads-N°45.
- ECCS. (1994), ECCS Manual on Design of Steel Structures in Seismic Zones, by F.M. Mazzolani and V. Piluso, TC 13 Seismic Design, N°76, Napoli, Italia.
- Elsati, M.K. and Richard, R.M. (1996), "Derived moment rotation curves for partially restrained connections", *Structural Engineering Review*, **8** (2/3), 151-158.
- Elnashai, A.S., Broderick, B.M. and Dowling, P.J. (1995), "Earthquake-resistant composite steel/concrete structures", *Struct. Eng.*, **73**(8), 121-132.
- Ermopoulos, J.C., Vayas, I., Petrovits, N.E., Sofianopoulos, D.S. and Spanos, C. (1995), "Cyclic behaviour of composite beam-to-column bolted joints", In *Steel Structures Eurosteel 95*, ed. A.N. Kounadis, A.A. Balkema, Rotterdam, pp. 205-210.
- Eurocode 3, ENV 1993-1-1. (1992), "Design of steel structures", CEN, European Committee for Standardization, Ref. No. ENV 1993-1-1: 1992, Brussels, Belgium.
- Eurocode 4, ENV 1994-1-1. (1996), "Proposed Annex J for EN 1994-1-1", Composite joints in building frames, CEN, European Committee for Standardization, Draft for meeting of CEN/TC 250/SC 4, Paper AN/57, Brussels, Belgium.
- Korol, R.M., Ghobarah, A. and Osman, A. (1990), "Extended end-plate connections under cyclic loading: behaviour and design", *J. Constr. Steel Res.*, **16**, 253-280.
- Lee, S.J. and Lu, L.W. (1989), "Cyclic tests of full-scale composite joints subassemblages", *J. Struct. Eng.*, **115**(8), 1977-1998.
- Leon, R.T. (1990), "Semi-rigid composite construction", *J. Constr. Steel Res.*, **15**, 99-120.
- Leon, R.T., Hajjar, J.F. and Gustafson, M.A. (1998), "Seismic response of composite moment-resisting connections", I: Performance. *J. Struct. Eng.*, **124**(8), 868-876.
- Leon, R.T., Hajjar, J.F. and Gustafson, M.A. (1998), "Seismic response of composite moment-resisting connections", II: Behaviour. *J. Struct. Eng.*, **124**(8), 877-885.
- Mazzolani, F.M. (1988), "Mathematical model for semi-rigid joints under cyclic loads", in R. BJORHOVDE et al. (eds) *Connections in Steel Structures: Behaviour, Strength and Design*, Elsevier Applied Science Publishers, London, 112-120.
- Plumier, A. (1994), "Behaviour of connections", *J. Constr. Steel Res.*, **29**, 95-119.
- Plumier, A. and Schleich, J.B. (1993), "Seismic resistance of steel and composite frame structures", *J. Constr. Steel Res.*, **27**, 159-176.
- Popov, E.P. (1988), "Seismic moment connections for MRFs", *J. Constr. Steel Res.*, **10**, 163-198.
- Pradhan, A.M. and Bouwkamp, J.G. (1994), "Structural performance aspects on cyclic behaviour of the composite beam-column joints", In *Behaviour of Steel Structures in Seismic Areas STESSA94*, ed. F.M. Mazzolani and V. Gioncu, E & FN SPON, London, pp. 221-230.
- Richard, R.M. and Abbott, B.J. (1975), "Versatile elasto-plastic stress-strain formula", *J. the Engineering Mechanics Division*, ASCE, **101**(EM4), 511-515.

Simões da Silva, L., Simões, R. and Cruz, P. (2001), "Behaviour of end-plate beam-to-column composite joints under monotonical loading", *Engineering Structures* (in print).

Simões, R.A.D. (2000), "Behaviour of beam-to-column composite joints under static and cyclic loading (in portuguese)", Ph.D Thesis, Civil Engineering Department, Universidade de Coimbra, Coimbra, Portugal.

## Nomenclature

$c$	Adjust parameter
$c_1$	Adjust parameter
$c_2$	Adjust parameter
$e_y$	Elastic displacement
$g$	Adjust parameter
$k$	Elastic initial stiffness
$k_a$	Elastic initial stiffness in the loading branch
$k_d$	Elastic initial stiffness in the unloading branch
$k_p$	Plastic final stiffness
$k_{pa}$	Plastic final stiffness in the loading branch
$k_{pd}$	Plastic final stiffness in the unloading branch
$p$	Adjust parameter
$s$	Adjust Parameter
$K_m$	Adjust Parameter
$K_y$	Elastic stiffness
$K_\phi$	Tangent stiffness relative to rotation $\phi$
$M$	Bending moment
$M'$	Bending moment in the beginning of the slippage branch
$M''$	Bending moment in the end of the slippage branch
$M_0$	Reference bending moment
$M_{0a}$	Reference bending moment
$M_{0d}$	Reference bending moment
$M_{0n}$	Reference bending moment in unloading branch
$M_{0p}$	Reference bending moment in loading branch
$M_1$	Reference bending moment
$M_2$	Reference bending moment
$M_{lim}$	Bending moment amplitude
$M_{lim0}$	$M_{lim}$ value in the first cycle
$M_n$	Reversal negative moment
$M_p$	Reversal positive moment
$M_y$	Elastic bending moment
$N$	Curve shape parameter
$R$	Stiffness at the start of each cycle
$R_0$	Tangent in the beginning of the first cycle obtained from the static monotonic moment-rotation results
$\varepsilon_i$	Resistance ratio
$f$	Total rotation of a joint
$\phi_{lim}$	Total rotation amplitude
$\phi_n$	Reversal negative rotation
$\phi_p$	Reversal positive rotation
$\phi_y$	Elastic rotation
$\eta_i$	Absorbed energy ratio
$\mu_i$	Full ductility
$\mu_{oi}$	Partial ductility
$\rho$	Parameter depending of bending moment in slippage branch

$\psi_i$	Full ductility ratio
$\Omega$	Accumulated energy at the end of the previous cycle
$\Omega_{\max}$	Accumulated energy at collapse
$\Delta M_{lim}$	Difference between $M_{lim}$ evaluated at the first and last cycle before collapse
$\Delta R$	Tangent variation between the first and last cycle before collapse
$\Delta\phi_s$	Slippage
$\Delta\phi_{s,\max}$	Slippage in the last cycle before failure
$\Delta\phi_{s,\min}$	Slippage in the first cycle
$CC$	